Exoskeleton Training Modulates Complexity in Movement Patterns and Cortical Activity in Able-Bodied Volunteers

Roberto Di Marco, *Member, IEEE*, Maria Rubega, *Member, IEEE*, Olive Lennon, Asja Vianello, Stefano Masiero, Emanuela Formaggio, and Alessandra Del Felice, on behalf of the PRO GAIT Consortium and Local Collaborators

***Abstract*— Robot-aided gait training (RAGT) plays a crucial role in providing high-dose and high-intensity task-oriented physical therapy. The human-robot interaction during RAGT remains technically challenging. To achieve this aim, it is necessary to quantify how RAGT impacts brain activity and motor learning. This work quantifies the neuromuscular effect induced by a single RAGT session in healthy middle-aged individuals. Electromyographic (EMG) and motion (IMU) data were recorded and processed during walking trials before and after RAGT. Electroencephalographic (EEG) data were recorded during rest before and after the entire walking session. Linear and nonlinear analyses detected changes in the walking pattern, paralleled by a modulation of cortical activity in the motor, attentive, and visual cortices immediately after RAGT. Increases in alpha and beta EEG spectral power and pattern regularity of the EEG match the increased regularity of body oscillations in the frontal plane, and the loss of alternating muscle activation during the gait cycle, when walking after a RAGT session. These preliminary results improve the understanding of human-machine interaction mechanisms and motor learning and may contribute to more efficient exoskeleton development for assisted walking.**

***Index Terms*— Robot-assisted gait training, motor learning, robotic rehabilitation, neuroplasticity, EEG, EMG, human–robot interaction.**

Manuscript received 19 December 2022; revised 24 March 2023; accepted 3 May 2023. Date of publication 8 May 2023; date of current version 25 May 2023. This study has been supported by a European Union-funded H2020 Research and Innovation Staff Exchange grant: PRO GAIT grant agreement No. 778043 (PRO GAIT project, www.progait.eu), and from the Italian Ministry for foreign Affairs and International Cooperation under grant No. PGR-01045 (SoftAct project). MR has been supported by REACT EU (Recovery Assistance for Cohesion and the Territories of Europe) - PON "Ricerca e Innovazione" 2014-2020", DM 1062/2021. *(Roberto Di Marco and Maria Rubega contributed equally to this work.) (Corresponding author: Maria Rubega.)*

This work involved human subjects or animals in its research. Approval of all ethical and experimental procedures and protocols was granted by the Ethics Committee of Treviso and Belluno: 'Comitato Etico per la Sperimentazione Clinica delle Province di Treviso e Belluno' under Application No. 725 CE/ORAS, and performed in line with the Declaration of Helsinki.

Roberto Di Marco was with the Department of Neurosciences, Section of Rehabilitation, University of Padova, 35128 Padua, Italy. He is now with the Department of Engineering for Innovation Medicine, University of Verona, 37134 Verona, Italy (e-mail: roberto.dimarco@univr.it).

Maria Rubega, Asja Vianello, and Emanuela Formaggio are with the Department of Neurosciences, Section of Rehabilitation, University of Padova, 35128 Padua, Italy (e-mail: maria.rubega@unipd.it; asja.vianello@gmail.com; emanuela.formaggio@unipd.it).

Olive Lennon is with the School of Public Health, Physiotherapy and Sports Science, University College Dublin, 4 Dublin, D04 V1W8 Ireland (e-mail: olive.lennon@ucd.ie).

Stefano Masiero is with the Department of Neurosciences, Section of Rehabilitation, University of Padova, 35128 Padua, Italy, and also with Ospedale Riabilitativo di Alta Specializzazione di Motta di Livenza, 31045 Motta di Livenza, Italy (e-mail: stef.masiero@unipd.it).

Alessandra Del Felice is with the Department of Neurosciences, Section of Neurology, University of Padova, 35128 Padua, Italy, and also with the Padova Neuroscience Center, University of Padova, 35129 Padua, Italy (e-mail: alessandra.delfelice@unipd.it).

This article has supplementary downloadable material available at https://doi.org/10.1109/TNSRE.2023.3273819, provided by the authors.

Digital Object Identifier 10.1109/TNSRE.2023.3273819

I. Introduction

ASSISTIVE devices, such as robots, support and enhance human performance and are already part of the industrial landscape. Assistive and rehabilitative robots have shown an important uptake in clinical and real world settings in the past decade, with a more widespread adoption projected in the next few years [1]. Clinical advantages include high intensity and high doses of therapeutic exercise. A limiting factor to robot uptake has been overcome by the introduction of wearable robots, – i.e., exoskeletons, which provide external support and integrate force generation of the user. Specifically, exoskeletons designed to train and assist gait have the advantage of allowing the user to walk in an ecological environment. In rehabilitation, robot-aided overground gait training (RAGT) can potentially enhance the confidence of users in navigating the environment, increasing neuroplasticity and strengthening motor learning [2], [3].

Robotic devices for overground gait rehabilitation allow for many repetitions of the gait cycle in a weight-bearing position and provide intense proprioceptive stimulation. It is also worth highlighting that RAGT relieves physiotherapists of supporting the user load [4], [5]. RAGT has shown clinical benefits in neurological diseases [5], [6]. For example, in stroke, people who undergo RAGT in the subacute stage demonstrate higher speed and endurance of walking, increased muscle strength, and a reorganization of the activation timing of lower limb muscles [5], [6]. What remains unclear is how neuroplasticity is modulated by RAGT. Compared to the wealth of studies focusing on clinical outcomes after RAGT, knowledge of

the neurophysiological phenomena underlying motor recovery following RAGT interventions remains poor [7]. Although RAGT induces modifications in cerebral and muscle activity in stroke survivors [8], [9], [10], [11], indicative of increased neural activity in the motor and associative areas of the brain, heterogeneity in the stratification of the participants and the protocols used limit clear conclusions at this time [12].

In stroke survivors, motor recovery should be paralleled by restoring cortical motor activity / networks where the slow rhythms of the affected hemisphere are recovered during the rehabilitation process [13]. Similarly, gross muscle co-contraction that affects gait smoothness and the physiological alternating cycling of stepping observed during hemiplegic gait may be concurrently addressed [14], [15].

Properly designed rehabilitation programs for gait recovery in clinical practice must be grounded on neurophysiological evidence, elucidating the type of neuromuscular reorganization provided by RAGT. The aim of this research is to identify the biomechanically-induced modifications on walking features, muscular activation patterns, and resting-state cortical activity induced by RAGT in able-bodied individuals. Our final aim is to investigate the determinants of any modifications observed. This information could help clarify how exoskeleton training modulates neuroplasticity and motor learning, and will provide an important building block required to develop more efficient and user-centered exoskeletons. Observed modifications induced by RAGT in able-bodied individuals can help inform the design of rehabilitative, assistive gait devices for people with neurological impairments.

Our research protocol design addressed the hypothesis that RAGT induces neuroplasticity and motor learning by: (i) a shift toward higher frequencies in sensorimotor areas after exoskeleton training; and (ii) changes in kinematic parameters, muscle activity, and timing modification of stride-synchronous pattern of muscle activation after RAGT.

II. Materials and Methods

The Materials and Methods section is detailed elsewhere [16], but we briefly report the relevant information hereinafter.

A. Participants

Ten able-bodied volunteers (5/5 M/F; age - median [1st quartile; 3rd quartile]: 47.1 [45.1; 48.8] years; height: 174.0 [169.3; 181.5] cm; body mass: 74.5 [67.3; 77.5] kg) with no reported neuro-muscular, cardiovascular, orthopedic or visual disorders were recruited. Data collection was carried out in accordance with the principles reported in the Declaration of Helsinki. The participants read and signed an informed consent, with full ethical approval granted by an Institutional Review Board (Treviso, PROGAIT TRAINER, 24.10.19).

B. Robotic Device

Among commercial devices on the market, the EKSO GT©(EKSObionics Inc., Richmond, CA, USA) consists of two lower limb supports connected to a torso equipped with a backpack, containing a battery and control electronics. The EKSO-user coupling is enabled by straps on the belly, both legs, and feet. Hip and knee joints are actuated in the sagittal plane, whereas the ankle has a single degree of freedom in the sagittal plane to facilitate the user from sitting to standing and vice versa. All other degrees of freedom are locked.

The EKSO is able to fully assist the user, providing enough power to perform the steps (*Full mode*), partially assist the user (*Adaptive mode*), considering his/her needs, or not assist the user (*Free mode* - where the actuators are off and the device supports its own weight). For device eligibility and safety, a user must be able to support his/her body weight using either a walking frame or crutches, transfer weight laterally and forward to allow the robot to initiate a forward step.

C. Measurement Systems

Participants were equipped with three wearable devices. Inertial Measurement Units (IMUs) consisting of a 3D accelerometer, a 3D gyroscope, and a magnetometer (Wave-Track Waterproof, Cometa srl, Milan, Italy). An IMU was placed on the fifth lumbar vertebra to follow the oscillation of the center of mass (COM) during gait and characterize its complexity and symmetry [17], [18], [19]. A waist-mounted IMU also served as a proxy to identify turnings from straight walking [20]. Two IMUs were placed laterally on the lower limb shanks to detect foot strike and foot off [21], to segment both lumbar acceleration and muscle activation signals.

Electromyography (EMG) was collected with a wireless EMG system (MiniWave Waterproof EMG sensors, Cometa srl, Milan, Italy) from the vastus lateralis (VL), biceps femoris (BF), tibialis anterior (TA) and gastrocnemius lateralis (GL) muscles of both legs [22], [23].

Activity of the Central Nervous System was collected with a wireless electroencephalographic (EEG) headset with 64 channels (g.NAUTILUS PRO system, g.tec medical engineering, Schiedlberg, Austria). An expert researcher identified the position of Cz based on the 10–20 measurements and gently scrubbed the scalp before placing the EEG cap and the gel, to maintain electrode-skin impedance $< 40k\Omega$. The gel was applied starting from the reference electrode (on the ear lobe), then the ground electrode, Cz, and all the other channels.

EEG, IMU and EMG data were collected synchronously through custom software C, using the g.NEEDACCESS.NET API (g.tec medical engineering, Schiedlberg, Austria) and the COMETA.NET API (Cometa srl, Milan, Italy). EEG and IMU data were collected at 250 Hz, whereas a 2000 Hz sampling frequency was used for EMG data. To ensure data synchronization among the three signals, EEG and IMU data were linearly upsampled to the lowest common multiple (i.e., 2000 Hz). More detail on this methodology is available in [16].

D. Data Collection Protocol

Each participant was asked to sit in a quiet environment with eyes open to collect a resting state EEG (pre-walking). The participants then walked, self-paced, on a 15 m corridor back and forth; we considered the first 15 m track as the baseline for the walking features.

Subsequently, they underwent a 30-minute gait training with an EKSO, mimicking usual clinical practice. The three modes

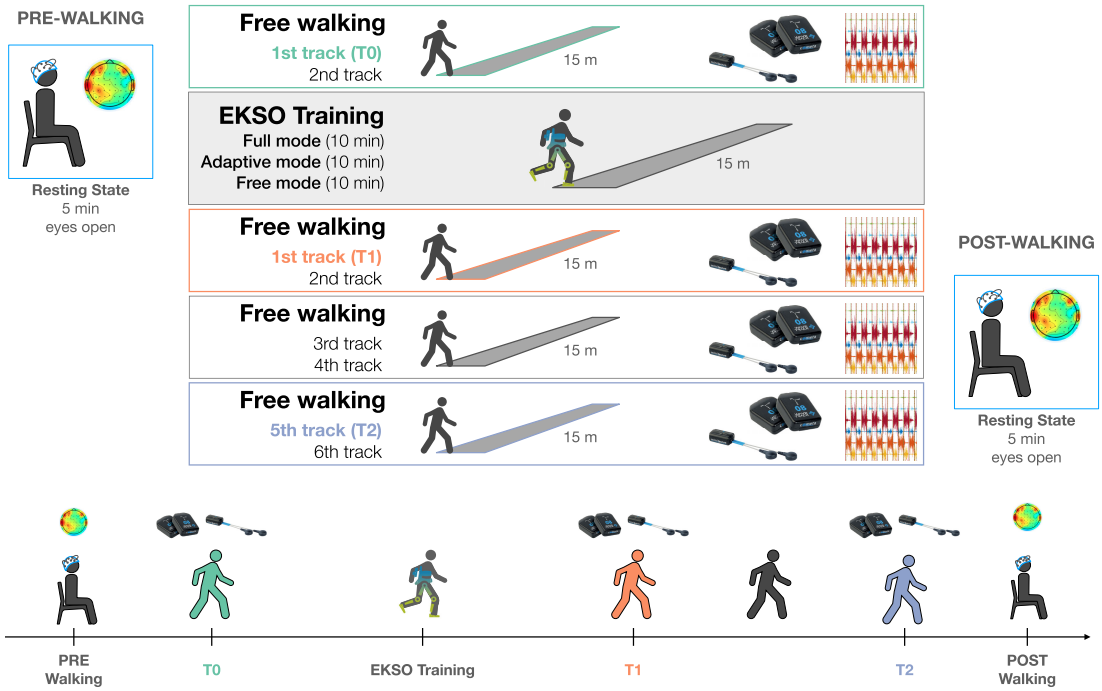

Fig. 1. Experimental protocol: (i) **Resting state recording pre-walking**: A 5-min resting state is recorded on the EEG while the participant is sitting with her/his eyes open, fixing a point in front of her/him, and slightly opening the mouth to relax facial muscles. (ii) **Free-walking recording**: the participant walks at a self-selected pace for 30 m (i.e., one trial: 15 m back and forth along the corridor). (iii) **EKSO walking training**: The participant walks with the EKSO device, programmed with the ProStep™ mode with three modalities (10 min each): Bilateral Max Assist mode, Adaptive Assist mode, Free mode. (iv) **Free-walking recording**. Three further walking trials (15 m back and forth each) are collected to observe whether there is a training effect or reestablishment of the baseline gait pattern after the EKSO removal. (v) **Resting state recording post-walking**: 5-min EEG resting state as in (i) was recorded at the end of the session.

of activation of the EKSO GT were deployed during this session (Fig. 1) [16].

Following EKSO training and deactivation of the device, participants again walked in a self-pace back and forth on the 15 m walkway three times – i.e., six tracks in total. We analyzed data from the first track traveled immediately after EKSO training (T1, light orange in Fig. 1) and from the fifth track as follow-up (T2, light blue in Fig. 1).

Lastly, a resting state EEG was again recorded (post-walking). The complete data collection procedure is summarized in Fig. 1 and detailed in [16].

E. Signal Processing

IMU data were downsampled from 2 kHz to 250 Hz, their actual sampling frequency, and then filtered, considering a 2^{nd} order low-pass Butterworth filter with a cutoff frequency equal to 6 Hz for the shin-mounted gyroscopes, and a 4^{th} order low-pass Butterworth filter with a cutoff frequency equal to 10 Hz for the other IMU signals.

To correct for possible misalignment of the sensor axes with the global anterior-posterior (AP), medial-lateral (ML) and vertical (VT – i.e., anti-parallel to gravity) directions of the body, a roll-pitch correction was estimated using the waist-mounted accelerometer as inclinometer from the initial standing condition, while participants are idling ahead of the "start" command and walk [24].

Turning onset and ending instants were estimated from the vertical component of the lumbar angular velocity [20], and only signals gathered from straight walking were retained for further analysis. Shin-mounted wearables served as a proxy for foot strikes and foot drops during gait and were used to calculate the spatiotemporal parameters of gait [21]. Gait events were used to calculate: the gait cycle duration, defined as the time interval, in seconds, between two subsequent foot strikes of the same foot; the step duration, i.e., the time interval in seconds between a foot strike and the foot strike of the contralateral foot; and cadence, calculated as the number of steps performed in a minute of walking. The walking speed was estimated by dividing the length of the walking track (15 m) by the time taken to cover that distance, determined by the gait events detected for the first step and the onset of the turning at the end of the corridor. In determining the spatiotemporal parameters of gait (except for average speed) and for the further analyses, the first and last strides of each walking 15 m track were discarded as they consisted of adjustment steps.

Lumbar acceleration in the AP, ML and VT directions was used to compute indices of overall gait symmetry and complexity, which we hypothesized would vary between pre- and post-training sessions.

Symmetry of gait was assessed with the improved Harmonic Ratio (iHR) [18]. The iHR is defined by relating the power of intrinsic harmonics (i.e., associated with the symmetric component of gait) to the total power of the signal for each stride, allowing a normalized index ranging from 0 (no symmetry) to 100% (total symmetry).

Complexity was assessed through Higuchi's algorithm that allows two parameters from a procedure that constructs sub-signals of different lengths from the original signal to be defined and checks whether subsignal patterns are repeated at different scales elsewhere in the original signal [25]. The more complex the signal, the higher the Higuchi's fractal dimension (HFD). The second parameter computed from with Higuchi's algorithm is the Tortuosity (τ_{ℓ_k}): a measure of the non-linear oscillatory behavior of the time-series. The greater the oscillatory components in the signal, the higher the tortuosity [26], [27], [28], [29]. EMG data were first filtered with a 4^{th} order band-pass Butterworth filter between 20 and 250 Hz [30], and then segmented stride-by-stride before further steps. For each muscle, we calculated the signal amplitudes (RMS) and Center of Activity throughout the gait cycle (CoA) [31], [32]. The CoA is the first trigonometric moment of the signal distribution. It has previously been used to compare muscle activity and timing under different conditions [32], as identifying all peak activity levels in major muscle groups may prove unreliable. The CoA was calculated using circular statistics (i.e., the `circ_mean` function in the CircStat Matlab toolbox [31]) on the envelope of the EMG time series for each muscle (i.e., the rectified and low-pass filtered (4^{th} order low-pass Butterworth filter, 10 Hz cutoff) time series), then time normalized on 201 points over each stride.

The co-contraction index (CCI) was calculated using the method originally described in [33] to evaluate the relative level of co-contraction between coupled agonist-antagonist muscles – i.e., VL-BF and TA-GL. A muscle contracts to provide action or stabilization to a human joint. As an example, when the foot hits the ground during walking, the action of the tibialis anterior prevents the foot from abrupt landing on the floor. However, an excessive contraction of TA in that gait phase would lead to an inefficient gait. Similarly, excessive co-contraction of the tibialis anterior (TA) and the gastrocnemius lateralis (GL) would lead to stiffening of the ankle joint [34], [35], and consequently to loss of fine movement control [36].

EEG data were zero phase high pass filtered above 1 Hz through a Butterworth filter of 4^{th} order and then zero phase low pass filtered below 40 Hz through a Butterworth filter of 4^{th} order avoiding phase distortion. 2-s non-overlapping EEG epochs were then extracted from the continuous dataset and individual epochs containing eye blinks and eye movements were also identified by visual inspection and removed from further analysis (average percentage of removed epochs: 40%). Data were cleaned from remaining physiological artifacts (remaining eye blinks, horizontal and vertical eye movements, muscle potentials, and other artifacts) through a Principal Component Analysis (PCA)-informed Independent Component Analysis (ICA) algorithm implemented in EEGLAB (average percentage of components removed: 10%).

We computed the absolute power spectra in the canonical EEG frequency bands, i.e., delta (1-4) Hz, theta (4-7) Hz, alpha (8-12) Hz, beta (14-24) Hz: (i) each 2-s EEG epoch was multiplied by a window function, i.e., Hamming window; (ii) the periodograms of all modified epochs were then averaged to estimate the power spectral density of each condition; (iii) the area under the curve (representing the power spectral density as a function of the frequency) was estimated for each EEG frequency band and represented by topographic maps.

For each EEG time-series in the scalp, both linear and non-linear features were assessed through Higuchi's algorithm. We refer the reader to [37] for further details on the application of HFD in EEG data. For each EEG time-series in the scalp, we applied the LAURA algorithm implemented in Cartool (cartoolcommunity.unige.ch) to calculate the source reconstruction, taking into account the age of the participants to calibrate the skull conductivity [38], [39]. The method restricts the solution space to the gray matter of the brain. The cortex was then parcellated into 83 brain regions of interest (ROIs). The dipoles in each ROI were represented with a unique time-series applying a singular value decomposition [40]. Absolute power spectra in the canonical EEG frequency bands were calculated for each ROI to estimate the sources in the cortex that were responsible for the different topographies in the scalp pre- and post-walking.

F. Statistical Analysis

All walking features were tested for differences between the three time points, that is, T0-T1-T2 (Fig. 1) – using a Friedman test and the Wilcoxon signed rank test paired as post hoc ($p_{value} = 0.05$). Effect size was calculated as the Z-statistic divided by the square root of the sample size [41].

To address the potential confounding factor of altered gait speed on the calculated walking features and muscle activity at the different time points, multiple linear regression models between these parameters and walking speed were run.

We performed two-sided, paired samples Wilcoxon signed-rank tests to compare power spectra and HFD values for each of the 64 EEG channels and 83 ROIs between pre- and post-walking trials (Fig. 1). Taking into account the limited sample size (10 participants), no corrections for multiple comparisons were made in the hypothesis testing.

III. Results

Due to the exploratory nature of this study and considering the relatively small sample size, Fig. 2–6 report significance obtained with Friedman and relevant post-hoc tests (no correction for multiple comparisons applied). When Friedman p_{value} is not given, post-hoc results should be interpreted as a trend towards significance, since their relevant effect size was large. Detailed p_{values} and effect sizes obtained for each statistical test are reported in the Supplemental Materials.

A. IMU Results

The analysis of the gait cycle parameters (Fig. 2) revealed a slight increase in the duration of the gait cycle between T0 and T1 (no significance), and a decrease in duration between T1 and T2 ($p_{value} = 0.0039$ for the left side – trend, and $p_{value} = 0.002$ for the right side). Coherent results were obtained for the stance phase (T0-T1 comparison: without significance; T1-T2:

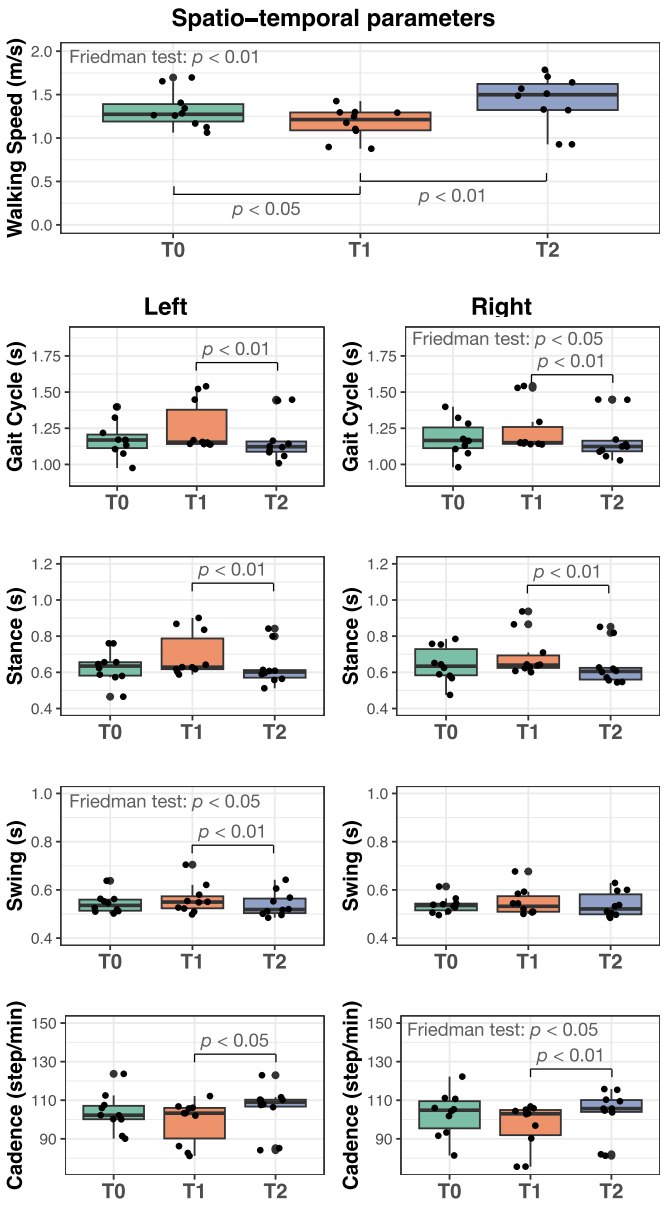

Fig. 2. Gait spatiotemporal parameters (that is, walking speed, gait cycle, stance, swing, cadence) calculated during the first free-walking track prior to the EKSO training (T0, green) and during the first free-walking track after the EKSO training (T1, orange) and the 5^{th} track (T2, light blue). The walking speed was estimated by dividing the length of the walking track – i.e., 15 m – by the time to cover that distance. The first column reports values for the left leg whilst the second column reports values for the right leg. Data are represented through boxplots reporting the minimum, maximum, sample median, and first and third quartiles. In each boxplot, *p*-values are reported for each Wilcoxon signed-rank test.

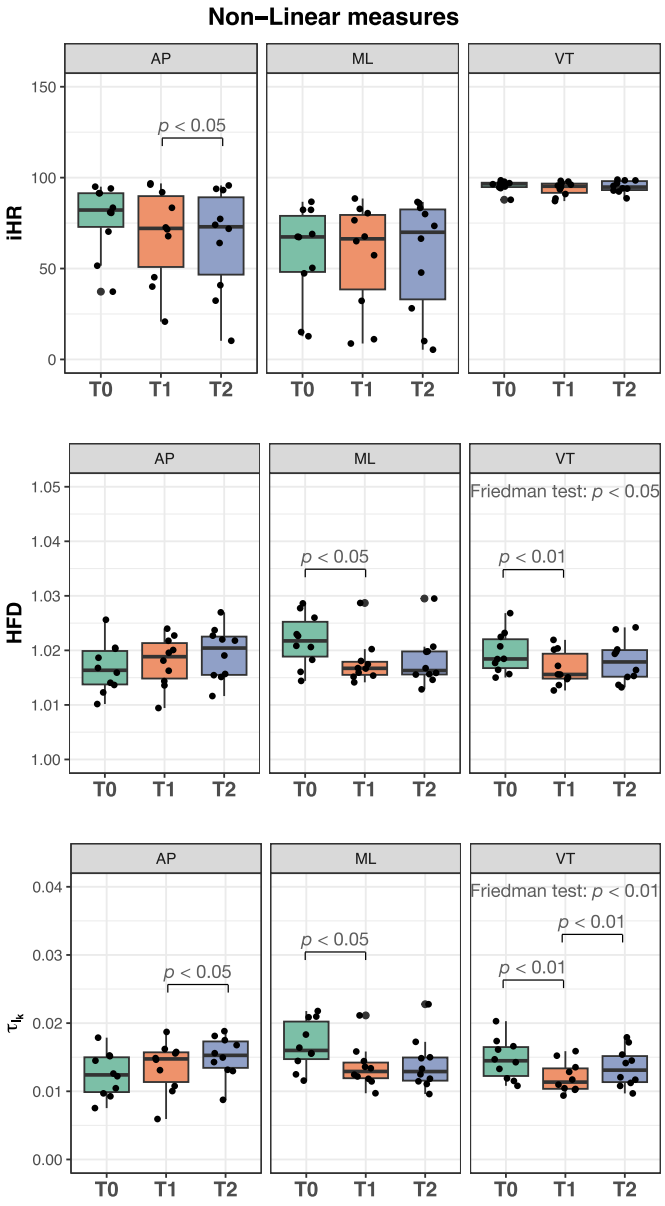

Fig. 3. Nonlinear metrics to quantify gait symmetry (improved Harmonic Ratio, iHR), complexity (Higuchi's Fractal Dimension, HFD) and periodicity (tortuosity, τ_{ℓ_k}) in the anterior-posterior (AP), medial-lateral (ML), and vertical (VT) directions of the body during walking. Nonlinear metrics were calculated during the first free-walking track prior to the EKSO training (T0, green) and during the first free-walking track after EKSO training (T1, orange) and the 5^{th} track (T2, light blue). p_{values} are reported for each Wilcoxon signed-rank test.

$p_{value} = 0.0039$ for the left and right sides, without significance for the Friedman test) and the duration of the swing phase (T0-T1 comparison: no significance; T1-T2: $p_{value} = 0.0059$ for the left side). Consistently, cadence (i.e., number of steps per minute - comparison T1-T2: $p_{value} = 0.02$ for the left side – trend, and $p_{value} = 0.0039$ for the right side) and walking speed, estimated considering a 15 m walking path and the time needed to travel that distance (T0-T1 comparison: $p_{value} = 0.019$; T1-T2: $p_{value} = 0.002$; T0-T2: without significance), decreased immediately after EKSO training and increased after the 5^{th} traveled walking track. No significance was identified in the comparisons T0-T2.

The symmetry of gait assessed via the iHR in all the inspected directions (AP, ML, and VT) did not change between the different time points (Fig. 3). A small trend was obtained for iHR between T1 and T2 in the AP direction ($p_{value} = 0.0488$), but with a non-significant omnibus Friedman test. Both Higuchi's fractal dimension (HFD) and tortuosity (τ_{ℓ_k}) calculated on lumbar acceleration revealed that no substantial modifications were induced in the gait pattern of the participants in the AP direction (Fig. 3). A significant difference was

observed only when comparing τ_{ℓ_k} at T1 and T2 ($p_{value} = 0.0371$), again with a non-significant Friedman test. Instead, the lumbar acceleration was less complex and less rich in oscillatory components immediately after EKSO training (that is, comparison T0-T1) in ML (HFD: $p_{value} = 0.0488$; τ_{ℓ_k}: $p_{value} = 0.0273$ – both with non-significant Friedman tests) and VT directions (HFD: $p_{value} = 0.0098$; τ_{ℓ_k}: $p_{value} = 0.002$), with τ_{ℓ_k} significant differences also observed between T1 and T2 in the VT direction ($p_{value} = 0.002$). See the Supplemental Materials for p_{value} and the effect size obtained for each comparison.

B. EMG Results

EMG data revealed a few statistically significant differences and some trends toward significance. In particular, the Root Mean Square (RMS, Fig. 4) increased between T1 and T2 for left BF ($p_{value} = 0.02$) and right BF ($p_{value} = 0.014$; with a significant Friedman test: $p = 0.045$), left GL ($p_{value} = 0.049$) and right TA ($p_{value} = 0.014$). A trend towards significantly increased RMS was also detected for the right GL between T0 and T1 ($p_{value} = 0.027$).

The Center of Activity (CoA) of the TA increased between T0 and T1 ($p_{value} = 0.037$) and between T0 and T2 ($p_{value} = 0.02$), with a positive Friedman test ($p_{value} = 0.0383$). This trend was also observed for the other muscle groups, though not significantly (Fig. 5A). Fig. 5B depicts the polar plots of the CoAs over the gait cycle percentage, clearly showing the reorganization of muscle activity in terms of timing between pre- and post-EKSO training. In particular, differences in muscle activity are observed in the gait cycle when comparing T0 with T1 and T2, in particular for the TA and GL muscles bilaterally (Fig. 5). No significant changes were observed between T1 and T2.

Co-contraction, as evaluated by the co-contraction index (CCI, Fig. 6), increased generally between pre and post EKSO training, with a significant difference obtained for the muscles of the right ankle (CCI_{TA-GL} – Friedman test: $p_{value} = 0.0383$; T0-T1 and T0-T2 comparisons: $p_{value} = 0.0098$).

Power of statistical results was generally small or moderate, however large effect sizes were obtained for those comparisons that returned significant differences (and a few additional comparisons on CoA). See the Supplemental Materials for detailed p_{value} and effect size.

C. Walking Features and Muscular Activity Correlation With Walking Speed

The Supplemental Materials reports detailed results of the linear regression models run between each calculated walking feature and muscular activity parameter and the walking speed, with relevant R^2 and p_{values}. These results highlight generally poor correlations, with a few statistically significace: i.e., RMS of the right BF, right TA and left GL; CCI of left VL-BF and TA-GL; CoA of the left TA; and HFD of lumbar acceleration in the AP direction ($p < 0.05$ and $0.40 < R^2 < 0.54$).

D. EEG Results

EEG power spectra changes following exoskeleton training (i.e., post-walking trial) reached statistical significance

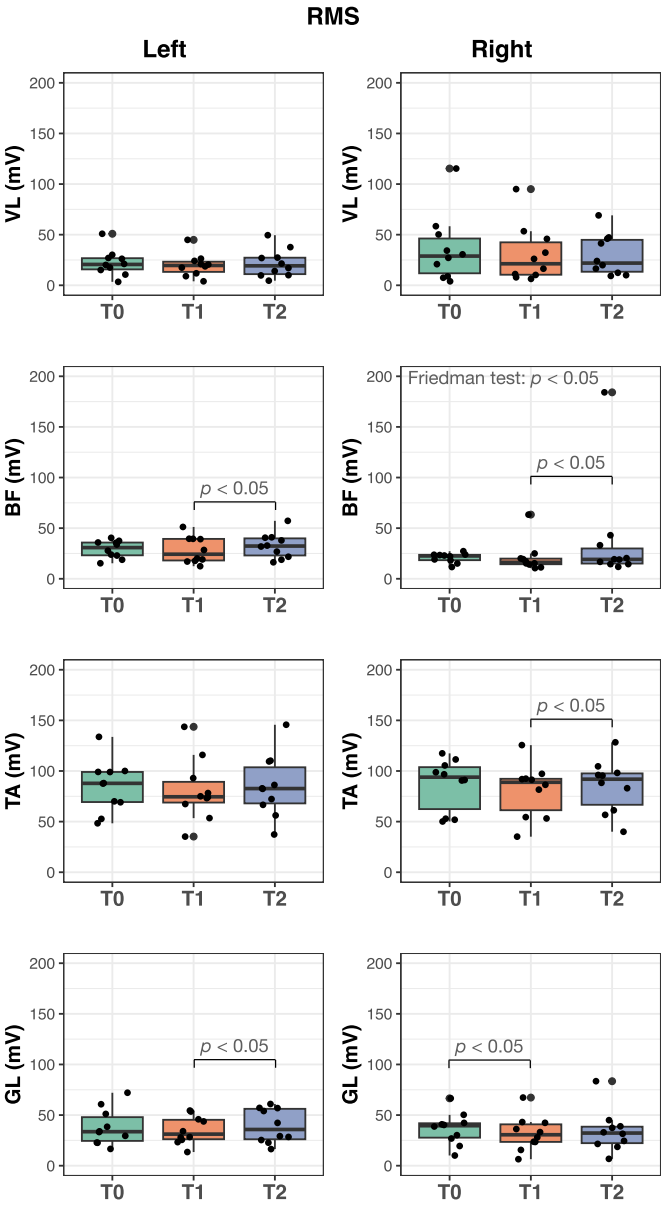

Fig. 4. Root Mean Square (RMS) calculated on electromyographic signals collected in the vastus lateralis (VL), biceps femoris (BF), tibialis anterior (TA), and gastrocnemius lateralis (GL) of both legs. RMS and CoA were calculated during the first free-walking track prior to the EKSO training (T0, green) and during the first free-walking track after the EKSO training (T1, orange) and the 5th track (T2, light blue). The first column reports values for the left leg while the second column reports values for the right leg. p_{values} are reported for each Wilcoxon signed-rank test.

(Fig. 7). During the 5-min pre-walking resting state recording (Fig. 7 (a-d)), as expected in a relaxed, stable, and comfortable state, the largest amplitudes in the alpha frequency range were evident in the parietal and occipital regions and the smallest in the frontal region, Fig. 7 (c). A significant statistical difference in spectral power was observed between EEG recordings pre- and post-walking trials in the sensorimotor brain areas, in both alpha and beta frequency bands Fig. 7 (m, n). Here, the average spectral power in alpha and beta increased after the exoskeleton training, Fig. 7 (g, h). In the lower EEG rhythms,

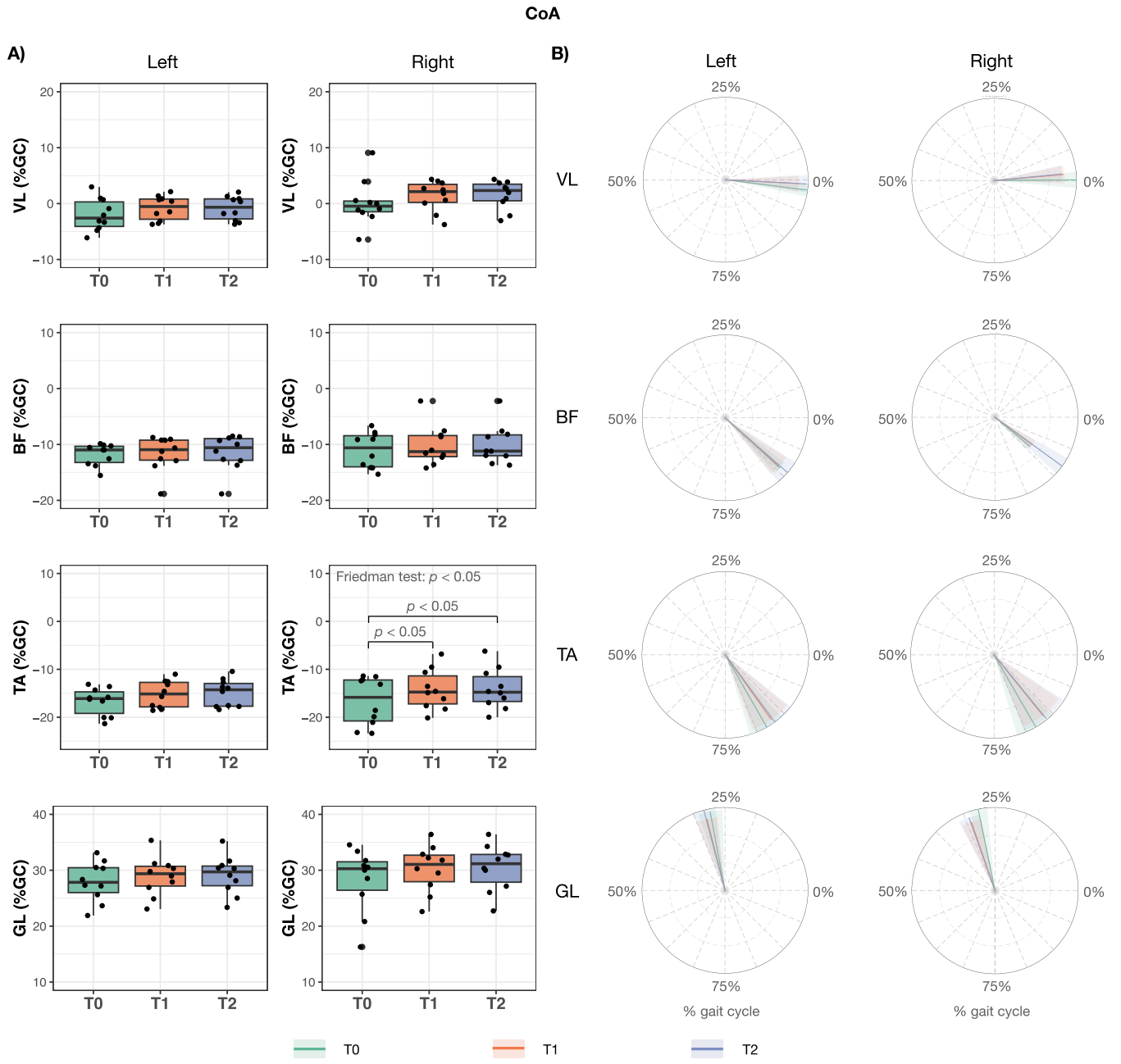

Fig. 5. Coefficient of Activity (CoA), presented as Boxplot (A) and Polar plots (B), of vastus lateralis (VL), biceps femoris (BF), tibialis anterior (TA), and gastrocnemius lateralis (GL) of both legs over the percentage of the gait cycle. (A) The first column reports values for the left leg, while the second column reports values for the right leg. p_{values} are reported for each Wilcoxon signed-rank test. (B) The radius of the polar sector is oriented as the mean CoA among participants; its length refers to the mean RMS, while its width refers to the mean angular standard deviation of CoA among participants. CoA was calculated during the first free-walking track before the EKSO training (T0, green) and during the first free-walking track after the EKSO training (T1, orange) and the fifth track (T2, light blue).

i.e., delta and theta, widespread differences between pre-Fig. 7 (a, b) and post-walking Fig. 7 (e, f) were not observed in Fig. 7 (i, l). These results are consistent with the increase in electrical source spectral power of: (a) Left Superior Parietal and Right Paracentral brain areas in delta frequency band; (b) Left and Right Rostral Anterior Cingulate and Right Enthorinal in theta frequency band; (c) Left Paracentral; Left Superior Parietal; Left and Right Precuneus; Right Lingual and Cuneus in alpha frequency band; (d) Left and Right Superior Parietal; Left Paracentral and Right Precuneus in beta frequency band, Fig. 8.

The complementary information resulted from nonlinear analysis, Fig. 9 (c), reports an increase in the regularity of EEG patterns in the parietal and occipital brain regions, i.e., HFD decreased in the post-walking trial, Fig. 9 (b), compared to pre-walking state, Fig. 9 (a).

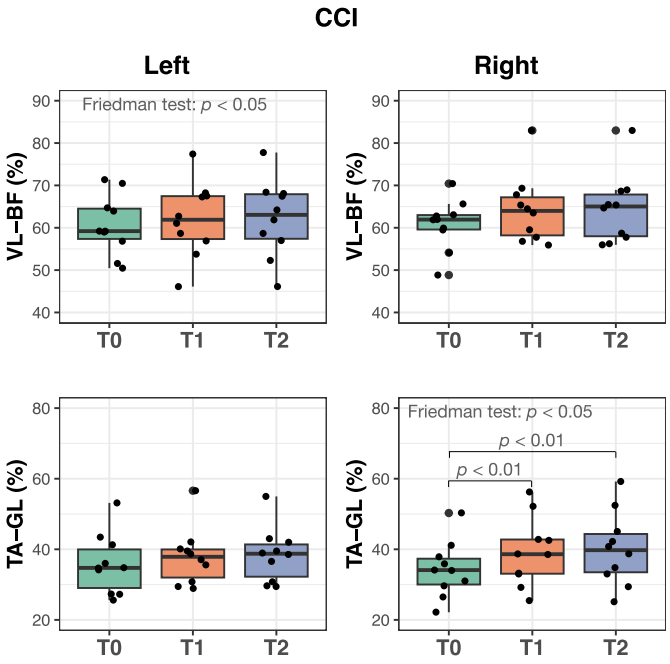

Fig. 6. Co-Contraction Index (CCI) calculated on electromyographical signals collected in antagonist muscles of the upper leg (vastus lateralis (VL) and biceps femoris (BF)), and lower leg (tibialis anterior (TA) and gastrocnemius lateralis (GL)) of both sides. CCI was calculated during the first free-walking track before the EKSO training (T0, green) and during the first free-walking track after the EKSO training (T1, orange) and the 5th track (T2, light blue). The first column reports values for the left leg, while the second column reports values for the right leg. p_{values} are reported for each Wilcoxon signed-rank test.

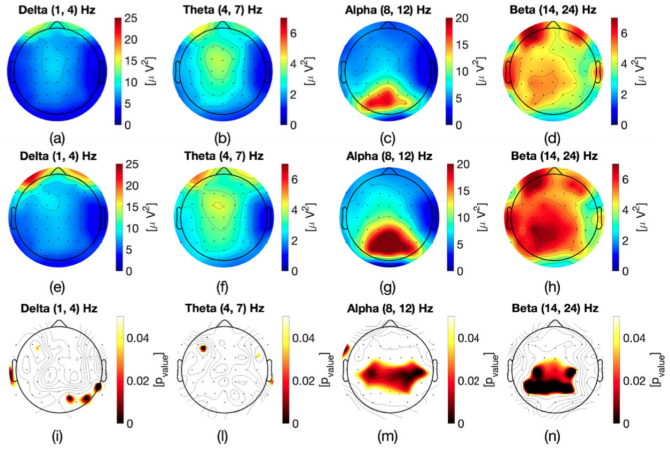

Fig. 7. Topography of the averaged value between participants in the power spectra (μV^2) in the canonical EEG frequency bands – i.e., (a, e) delta (1-4) Hz; (b, f) theta (4-7) Hz; (c, g) alpha (8-12) Hz; (d, h) beta (14-24) Hz – (a, b, c, d) pre and (e, f, g, h) post-walking. (i, l, m, n) Statistical maps reporting the p-value of the statistically significant difference between the differences in the EEG power spectra in each frequency band, assessed by a two-sided sign-test.

IV. Discussion

Our knowledge of human-robot interaction, particularly in the context of robot-assisted walking, remains limited. Therefore, the aim of this exploratory study was to provide a granular description of the muscular and cortical modifications induced by a single session of RAGT in able-bodied individuals. This knowledge is imperative as a foundation to design assistive and rehabilitation robotic devices.

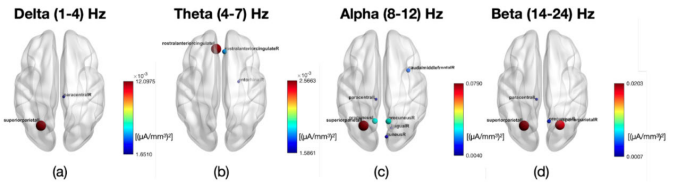

Fig. 8. Averaged values (between participants) of the difference in power spectra in the source domain between post- and pre-walking trials in the canonical frequency bands. Only values that statistically resulted significant are reported: (a) Left Superior Parietal and Right Paracentral brain areas in delta band; (b) Left and Right Rostral Anterior Cingulate and Right Enthorinal in theta; (c) Left Paracentral; Left Superior Parietal; Left and Right Precuneus; Right Lingual and Cuneus in alpha; (d) Left and Right Superior Parietal; Left Paracentral and Right Precuneus in beta. The dimension and color of the node (centered on each ROI) identify the value of the power difference ($(\mu A/mm^3)^2$) of the reconstructed source waveforms under the two conditions. Brain networks were visualized with the BrainNet Viewer [42].

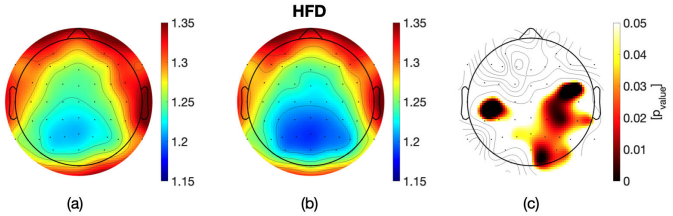

Fig. 9. Topography of the average value between participants of the Fractal Dimension (HFD) of Higuchi (a) pre- and (b) post-walking. (c) Statistical map reporting the p-value of the statistical significant difference between HFD differences between pre and post, assessed by two-sided sign-test.

In our experiment, sensorimotor rhythms, namely alpha and beta, increased at the end of the training session, a finding mirrored by an increase in EEG signal regularity measured with Higuchi's fractal dimension (HFD). Similarly, HFD and tortuosity (τ_{ℓ_k}), calculated on IMUs signal, showed a lower complexity (i.e., higher regularity) of the lumbar acceleration in the mediolateral and vertical directions after EKSO training. These changes in kinematics suggest a modulation of self-paced overground walking towards a more periodic pattern. This could be a carryover effect. EMG signal analysis highlighted a higher activation of a subset of lower limb muscles and a loss of the physiological sequential timing of activation throughout the gait cycle. Although only a few significances for CoA were obtained at different time points (i.e., T0-T1-T2) for the left and right lower limbs, statistics returned small to moderate power for the majority of our comparisons at T0-T1 and T0-T2 for RMSs, CoAs and CCIs (see Supplemental Materials). This suggests that a larger sample size would help generalize the results, and possibly support finding more significant differences where only a trend can currently be observed.

These modulations in neurophysiological and motor patterns could be a manifestation of motor learning. Indeed, although the walking speed is known to affect walking features, correlation of speed with the other walking features and muscular activity parameters was poor ($p < 0.05$ and $0.40 < R^2 < 0.54$), thus not explaining the differences among the results. RAGT may have acted as a motor priming,

i.e., a non-conscious learning process which occurs when the exposure to a first stimulus changes the response to a subsequent stimulus [43].

The observed modifications could reflect pure motor learning, with strong extrinsic feedback provided by the mechanical constraint [44] over a limited timescale. We observed an increase in the activity of the frontal midline theta (FMT), located at the source level in Left and Right Rostral Anterior Cingulate and Right Enthorinal after robotic gait training. In cognitive control tasks, FMT oscillations (4–8 Hz) are frequent [45]. FMT oscillations have been associated with cognitive effort [46], described as the strain of continuously summoning cognitive control.

Our data suggest an increased cognitive effort induced by RAGT. This may have been expected, in part, since all participants were naive to the device. Quantification of this induced mental workload might increase the effectiveness of training, allowing the intensity of the training to be adapted to a level that promotes motor learning [47] without challenging the subject to a non-efficient level of physical and mental exertion in a known trade-off. In fact, motor learning has been shown to be promoted by cognitively challenging, though not distressing, tasks [47]. Despite an increased interest in this topic, to our knowledge up to now only a few studies, based on prosthetics, focused on changes in brain activity (i.e., change in spectral power of the alpha and theta bands) related to cognitive load [48] during gait training. Brain activity reflects purely cognitive effort and is therefore considered a more appropriate physiological measure to quantify this aspect of training during RAGT.

Another finding we observed in this study was an increase in alpha rhythm in the occipital areas. This activity might be interpreted as increased visual activation due to the complex spatial navigation task of exoskeleton overground training. This additional cortical activation, while adding to the cognitive effort, stresses also a particular advantage of exoskeleton gait training among RAGT technologies, where training takes place in an ecological environment and provides an enriched rehabilitation experience that is not limited to a treadmill.

Our findings must be interpreted considering a few limitations. This study did not include subjective measures of cognitive and physical exertion associated with self-selected overground walking and RAGT. This aim was beyond the scope of our study when we designed the protocol. There is a lack of standardized tools for these assessments, which would have made these evaluations challenging. Standardized agreement on core outcomes and additional research is required in this field. Another limitation, given the exploratory nature of the study, is the small sample size, which provided significant results.

The idea behind this research was to study what mechanisms are induced in able-bodied subjects with the use of a RAGT device. Furthermore, differently from what is proposed in this study, considering only one activation mode for the RAGT device could help to further distinguish which mode of use should be preferred to specifically treat different medical conditions. Another limitation may be the relatively short follow-up, which hinders us from quantification of the duration of the short-term plasticity after-effects of RAGT.

V. Conclusion

Our data provide evidence of a priming and motor learning effect achieved in a single session of robotic gait training. The gait pattern of overground-free walking immediately after a RAGT session is characterized by an increase in regularity and periodicity in the frontal plane, paralleled by greater activation and a loss of sequential physiological timing of the lower leg muscles during the gait cycle. These features probably represent a carryover effect of robotic gait, which diminishes within a few minutes after RAGT.

These data prevent us from any speculation on the possible neuromuscular induced activation in neurological populations. These preliminary findings point to overlooked aspects of robotic gait training. It appears that physiological corticospinal activity after overground free gait in able-bodied subjects cannot be compared with that obtained after robotic training in the same sample. This observation stresses the need to build repositories of neurophysiological and kinematic data recorded during RAGT to be used as reference data for clinical studies.

Acknowledgment

Members of the PRO GAIT Consortium (in alphabetic order): Ekso Bionics Inc., USA: Katherine Strausser. g.tec Medical Engineering GmbH, Austria: Christoph Guger, Rupert Ortner. Mater Misericordiae University Hospital, Ireland: Caitriona Fingleton, Sean Murphy. Ulster University, U.K.: Damien Coyle. Villa Beretta Rehabilitation Center, Valduce Hospital, Italy: Eleonora Guanziroli, Franco Molteni.

Local Collaborators (in alphabetic order): Ospedale Riabilitativo di Alta Specializzazione di Motta di Livenza, Italy: Ilenia Bonini, Humberto Antonio Cerrel Bazo, Francesco Faliero, Paolo Pauletto. University of Padova, Italy: Giacomo Dazzi, Chiara Venturin.

References

[1] A. Rodríguez-Fernández, J. Lobo-Prat, and J. M. Font-Llagunes, "Systematic review on wearable lower-limb exoskeletons for gait training in neuromuscular impairments," *J. NeuroEng. Rehabil.*, vol. 18, no. 1, pp. 1–21, Dec. 2021.

[2] A. De Luca et al., "Exoskeleton for gait rehabilitation: Effects of assistance, mechanical structure, and walking aids on muscle activations," *Appl. Sci.*, vol. 9, no. 14, p. 2868, Jul. 2019.

[3] G. Morone et al., "Robot-assisted gait training for stroke patients: Current state of the art and perspectives of robotics," *Neuropsychiatric Disease Treatment*, vol. 13, p. 1303, May 2017.

[4] D. R. Louie and J. J. Eng, "Powered robotic exoskeletons in post-stroke rehabilitation of gait: A scoping review," *J. NeuroEng. Rehabil.*, vol. 13, no. 1, pp. 1–10, Dec. 2016.

[5] E. Hoyer, A. Opheim, and V. Jorgensen, "Implementing the exoskeleton Ekso GT^{TM} for gait rehabilitation in a stroke unit—Feasibility, functional benefits and patient experiences," *Disab. Rehabil., Assistive Technol.*, vol. 17, no. 4, pp. 473–479, May 2022.

[6] M. Maier, B. R. Ballester, and P. F. M. J. Verschure, "Principles of neurorehabilitation after stroke based on motor learning and brain plasticity mechanisms," *Frontiers Syst. Neurosci.*, vol. 13, p. 74, Dec. 2019.

[7] A. Berger et al., "Increased gait variability during robot-assisted walking is accompanied by increased sensorimotor brain activity in healthy people," *J. NeuroEng. Rehabil.*, vol. 16, no. 1, pp. 1–13, Dec. 2019.

[8] S. Y. Shin, K. Hohl, M. Giffhorn, L. N. Awad, C. J. Walsh, and A. Jayaraman, "Soft robotic exosuit augmented high intensity gait training on stroke survivors: A pilot study," *J. NeuroEng. Rehabil.*, vol. 19, no. 1, pp. 1–12, Jun. 2022.

[9] F. Molteni et al., "Brain connectivity modulation after exoskeleton-assisted gait in chronic hemiplegic stroke survivors: A pilot study," *Amer. J. Phys. Med. Rehabil.*, vol. 99, no. 8, pp. 694–700, 2020.

[10] P. Caliandro et al., "Exoskeleton-assisted gait in chronic stroke: An EMG and functional near-infrared spectroscopy study of muscle activation patterns and prefrontal cortex activity," *Clin. Neurophysiol.*, vol. 131, no. 8, pp. 1775–1781, Aug. 2020.

[11] R. S. Calabro et al., "Shaping neuroplasticity by using powered exoskeletons in patients with stroke: A randomized clinical trial," *J. NeuroEng. Rehabil.*, vol. 15, no. 1, pp. 1–16, Dec. 2018.

[12] O. Lennon et al., "A systematic review establishing the current state-of-the-art, the limitations, and the DESIRED checklist in studies of direct neural interfacing with robotic gait devices in stroke rehabilitation," *Frontiers Neurosci.*, vol. 14, p. 578, Jun. 2020.

[13] M. Gandolfi et al., "Quantification of upper limb motor recovery and EEG power changes after robot-assisted bilateral arm training in chronic stroke patients: A prospective pilot study," *Neural Plasticity*, vol. 2018, pp. 1–15, Jan. 2018.

[14] V. Weerdesteyn, M. D. Niet, H. J. R. van Duijnhoven, and A. C. H. Geurts, "Falls in individuals with stroke," *J. Rehabil. Res. Develop.*, vol. 45, no. 8, pp. 1195–1214, 2008.

[15] V. Longatelli, A. Pedrocchi, E. Guanziroli, F. Molteni, and M. Gandolla, "Robotic exoskeleton gait training in stroke: An electromyography-based evaluation," *Frontiers Neurorobotics*, vol. 15, pp. 1–13, Nov. 2021.

[16] R. Di Marco et al., "Experimental protocol to assess neuromuscular plasticity induced by an exoskeleton training session," *Methods Protocols*, vol. 4, no. 3, p. 48, Jul. 2021.

[17] M. D. Latt, H. B. Menz, V. S. Fung, and S. R. Lord, "Acceleration patterns of the head and pelvis during gait in older people with Parkinson's disease: A comparison of fallers and nonfallers," *Journals Gerontol. Ser. A, Biol. Sci. Med. Sci.*, vol. 64, no. 6, pp. 700–706, Jun. 2009.

[18] I. Pasciuto, E. Bergamini, M. Iosa, G. Vannozzi, and A. Cappozzo, "Overcoming the limitations of the harmonic ratio for the reliable assessment of gait symmetry," *J. Biomechanics*, vol. 53, pp. 84–89, Feb. 2017.

[19] M. C. Bisi, P. Tamburini, and R. Stagni, "A 'fingerprint' of locomotor maturation: Motor development descriptors, reference development bands and data-set," *Gait Posture*, vol. 68, pp. 232–237, Feb. 2019.

[20] M. El-Gohary et al., "Continuous monitoring of turning in patients with movement disability," *Sensors*, vol. 14, no. 1, pp. 356–369, 2014.

[21] A. Salarian et al., "Gait assessment in Parkinson's disease: Toward an ambulatory system for long-term monitoring," *IEEE Trans. Biomed. Eng.*, vol. 51, no. 8, pp. 1434–1443, Aug. 2004.

[22] Y. Blanc and U. Dimanico, "Electrode placement in surface electromyography (sEMG) 'Minimal Crosstalk Area' (MCA)," *Open Rehabil. J.*, vol. 3, no. 1, pp. 110–126, 2010.

[23] J. V. Basmajian, "Electrode placement in electromyographic biofeedback," in *Biofeedback: Principles and Practice for Clinicians*. Baltimore, MD, USA: Williams & Wilkins, 1983.

[24] R. Moe-Nilssen, "A new method for evaluating motor control in gait under real-life environmental conditions. Part 2: Gait analysis," *Clin. Biomechanics*, vol. 13, nos. 4–5, pp. 328–335, Jun. 1998.

[25] T. Higuchi, "Approach to an irregular time series on the basis of the fractal theory," *Phys. D, Nonlinear Phenom.*, vol. 31, no. 2, pp. 277–283, 1988.

[26] F. Finotello, F. Scarpa, and M. Zanon, "EEG signal features extraction based on fractal dimension," in *Proc. 37th Annu. Int. Conf. IEEE Eng. Med. Biol. Soc. (EMBC)*, Aug. 2015, pp. 4154–4157.

[27] F. Scarpa, M. Rubega, M. Zanon, F. Finotello, A.-S. Sejling, and G. Sparacino, "Hypoglycemia-induced EEG complexity changes in type 1 diabetes assessed by fractal analysis algorithm," *Biomed. Signal Process. Control*, vol. 38, pp. 168–173, Sep. 2017.

[28] M. Rubega, F. Scarpa, D. Teodori, A.-S. Sejling, C. S. Frandsen, and G. Sparacino, "Detection of hypoglycemia using measures of EEG complexity in type 1 diabetes patients," *Entropy*, vol. 22, no. 1, p. 81, Jan. 2020.

[29] R. Di Marco, M. Rubega, A. Antonini, E. Formaggio, S. Masiero, and A. Del Felice, "Fractal analysis of lower back acceleration profiles in balance tasks," in *Proc. 43rd Annu. Int. Conf. IEEE Eng. Med. Biol. Soc. (EMBC)*, Nov. 2021, pp. 7381–7384.

[30] A. Merlo and I. Campanini, "Applications in movement and gait analysis," in *Surface Electromyography: Physiology, Engineering, and Applications*. Hoboken, NJ, USA: Wiley, 2016, pp. 440–459.

[31] P. Berens, "CircStat: A MATLAB toolbox for circular statistics," *J. Stat. Softw.*, vol. 31, no. 10, pp. 1–21, 2009.

[32] F. Sylos-Labini et al., "EMG patterns during assisted walking in the exoskeleton," *Frontiers Hum. Neurosci.*, vol. 8, p. 423, Jun. 2014.

[33] K. Falconer and D. Winter, "Quantitative assessment of co-contraction at the ankle joint in walking," *Electromyogr. Clin. Neurophysiol.*, vol. 25, nos. 2–3, pp. 135–149, 1985.

[34] I. Campanini, A. Merlo, and B. Damiano, "A method to differentiate the causes of stiff-knee gait in stroke patients," *Gait Posture*, vol. 38, no. 2, pp. 165–169, 2013.

[35] A. Merlo and I. Campanini, "Impact of instrumental analysis of stiff knee gait on treatment appropriateness and associated costs in stroke patients," *Gait Posture*, vol. 72, pp. 195–201, Jul. 2019.

[36] M. Rubega et al., "Cortical correlates in upright dynamic and static balance in the elderly," *Sci. Rep.*, vol. 11, p. 15, Jul. 2021.

[37] M. Rubega et al., "EEG fractal analysis reflects brain impairment after stroke," *Entropy*, vol. 23, no. 5, p. 592, May 2021.

[38] L. Spinelli, S. A. Gonzales, G. Lantz, M. Seeck, and C. M. Michel, "Electromagnetic inverse solutions in anatomically constrained spherical head models," *Brain Topography*, vol. 13, no. 2, pp. 115–125, 2000.

[39] C. M. Michel and D. Brunet, "EEG source imaging: A practical review of the analysis steps," *Frontiers Neurol.*, vol. 10, p. 325, Apr. 2019.

[40] M. Rubega et al., "Estimating EEG source dipole orientation based on singular-value decomposition for connectivity analysis," *Brain Topography*, vol. 32, no. 4, pp. 704–719, Jul. 2019.

[41] M. Tomczak and E. Tomczak, "The need to report effect size estimates revisited. An overview of some recommended measures of effect size," *Trends Sport Sci.*, vol. 21, no. 1, pp. 1–7, 2014.

[42] M. Xia, J. Wang, and Y. He, "BrainNet viewer: A network visualization tool for human brain connectomics," *PLoS ONE*, vol. 8, no. 7, Jul. 2013, Art. no. e68910.

[43] M. E. Stoykov, D. M. Corcos, and S. Madhavan, "Movement-based priming: Clinical applications and neural mechanisms," *J. Motor Behav.*, vol. 49, no. 1, pp. 88–97, Jan. 2017.

[44] R. A. Schmidt, "Frequent augmented feedback can degrade learning: Evidence and interpretations," in *Tutorials in Motor Neuroscience*. Berlin, Germany: Springer, 1991, pp. 59–75.

[45] T. Gebuis, W. Gevers, and R. C. Kadosh, "Topographic representation of high-level cognition: Numerosity or sensory processing?" *Trends Cognit. Sci.*, vol. 18, no. 1, pp. 1–3, Jan. 2014.

[46] A. Westbrook and T. S. Braver, "Cognitive effort: A neuroeconomic approach," *Cognit., Affect., Behav. Neurosci.*, vol. 15, no. 2, pp. 395–415, Jun. 2015.

[47] A. Kaelin-Lang, L. Sawaki, and L. G. Cohen, "Role of voluntary drive in encoding an elementary motor memory," *J. Neurophysiol.*, vol. 93, no. 2, pp. 1099–1103, Feb. 2005.

[48] S. Möller, D. Rusaw, K. Hagberg, and N. Ramstrand, "Reduced cortical brain activity with the use of microprocessor-controlled prosthetic knees during walking," *Prosthetics Orthotics Int.*, vol. 43, no. 3, pp. 257–265, 2019.

Open Access funding provided by 'Università degli Studi di Padova' within the CRUI CARE Agreement